ACS APPLIED MATERIALS & INTERFACES

Research Article

www.acsami.org

$ZnSe{\cdot}0.5N_2H_4$ Hybrid Nanostructures: A Promising Alternative Photocatalyst for Solar Conversion

Yu-Chih Chen,[†] Tao-Cheng Liu,[†] and Yung-Jung Hsu*

Department of Materials Science and Engineering, National Chiao Tung University, 1001 University Road, Hsinchu, Taiwan 30010, Republic of China

Supporting Information

ABSTRACT: As the molecular precursor of ZnSe, $ZnSe{\cdot}0.5N_2H_4$ inorganic–organic hybrids have received relatively less attention due to the feasibility of their further processing and decomposition into pure-phase ZnSe. Here we demonstrated that $ZnSe{\cdot}0.5N_2H_4$ hybrid nanostructures, which were prepared using a facile hydrazine-assisted hydrothermal method, may practically harvest solar energy for photoconversion applications. By modulating the volume ratio of hydrazine hydrate to deionized water employed in the synthesis, the morphology of the grown $ZnSe{\cdot}0.5N_2H_4$ can be varied, which included nanowires, nanobelts and nanoflakes. With the relatively long exciton lifetime and highly anisotropic structure, $ZnSe{\cdot}0.5N_2H_4$ nanowires performed much better in the photodegradation of rhodamine B than the other two counterpart products. As compared to pure ZnSe nanoparticles and single-phase ZnSe nanowires obtained from further processing $ZnSe{\cdot}0.5N_2H_4$, the $ZnSe{\cdot}0.5N_2H_4$ hybrid nanowires exhibited superior photocatalytic performance under visible light illumination. The hybrid nanowires were further decorated with Au particles to endow them with structural and compositional diversities. Time-resolved photoluminescence spectra suggested that almost 40% of the photoexcited electrons in $ZnSe{\cdot}0.5N_2H_4$ nanowires can be transported to the decorated Au, which enabled a fuller extent of participation of charge carriers in the photocatalytic process and thus conduced to a significant enhancement in the photocatalytic activity. The demonstrations from this work illustrate that $ZnSe{\cdot}0.5N_2H_4$ hybrid nanostructures can serve as a versatile photocatalyst platform for advanced photocatalytic applications.

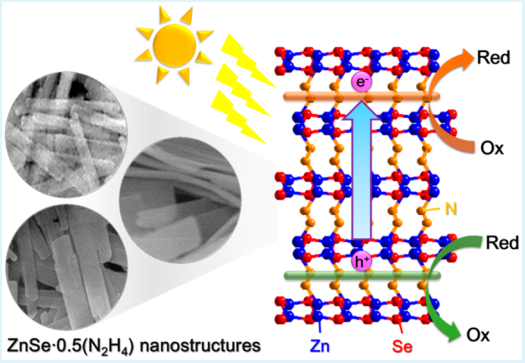

KEYWORDS: *$ZnSe{\cdot}0.5N_2H_4$, inorganic–organic hybrids, photocatalysis, solar energy conversion*

INTRODUCTION

Inorganic–organic hybrid nanostructures have garnered appreciable attention in the past few years because they may exhibit superior material properties that are difficult to acquire from either inorganic or organic materials alone.[1] The organic substance not only tailors the physical properties of the inorganic constituent by intercalating into its framework but also enriches the chemical diversities of the structures through imposing specific functional groups.[2,3] Of particular interest are the semiconductor-based hybrid nanostructures, which have been regarded as a prospective photocatalyst paradigm as a result of the synergy between the constituents.[4] So far, various kinds of inorganic–organic semiconductor-based composites have been proposed and developed, such as $ZnSe{\cdot}N_2H_4$ nanobelts,[5] ZnSe·0.5(EN) nanoplates, nanoribbons, and nanoflowers (EN = ethylenediamine),[6−8] ZnS·0.5(EN) nanosheets,[9] ZnSe·0.5(DETA) nanobelts (DETA = diethylenetriamine),[10] $ZnTe{\cdot}2N_2H_4$ polymorphs,[11] ZnSe·0.5(TEPA) nanostructures (TEPA = tetraethylenepentamine),[12] and CdE·0.5(EN) nanostructures (E = S, Se, Te).[13,14] These developments have witnessed a rising demand for the rational design of inorganic–organic hybrid nanostructures to further the advancement of materials science.

Hydrothermal process represents a facile and effective method for the preparation of inorganic–organic hybrid nanostructures. In the typical procedure, a specific organic substance is employed as the stabilizer for the reaction species and functions as the intercalation molecule for the composite structure formation.[15] For example, for the preparation of ZnSe·0.5(EN) nanoplates,[6] EN molecules first coordinate Zn^{2+} ions to generate Zn^{2+}-EN complex. The Se^{2-} ions then react with the Zn^{2+}-EN complex to form ZnSe layered structure with EN molecules orderly intercalated between the slabs. Noticeably, the intercalated EN of ZnSe·0.5(EN) can be further removed with a post-heat treatment or a secondary hydrothermal reaction,[8,16] which results in the formation of pure-phase ZnSe. Because of the feasibility of their further processing to form pure-phase semiconductor, inorganic–organic semiconductor-based composites themselves have received relatively less attention. Most studies concerning these hybrid nanostructures mainly explored the structural characteristics and optical properties, and their applicability in practical situations is still

Received: October 14, 2014
Accepted: December 26, 2014
Published: December 26, 2014

DOI: 10.1021/am507085u
ACS Appl. Mater. Interfaces 2015, 7, 1616−1623

not widely reported. Since the inorganic−organic semiconductor-based hybrid nanostructures may inherit the fundamental properties of the semiconductor component, one may expect promising optoelectronic applications for these composites, especially in the practical photoconversion processes, although it has not been well-addressed thus far.

In this work, we presented a hydrazine-assisted hydrothermal process for the controlled growth of inorganic−organic ZnSe·$0.5N_2H_4$ hybrid nanostructures. The synthesis used $ZnCl_2$ and Se powder as the precursors and a mixed solution of deionized water and hydrazine hydrate ($N_2H_4·H_2O$) as the reaction medium. The organic ligand N_2H_4 not only acted as an intercalation molecule for the formation of hybrid nanostructures but also functioned as the molecular template to dictate the product morphology. By suitably modulating the volume ratio of hydrazine hydrate to deionized water employed, the composition and morphology of the resultant nanostructures can be tailored. The products included ZnSe nanoparticles, ZnSe·$0.5N_2H_4$ hybrid nanowires, ZnSe·$0.5N_2H_4$ hybrid nanobelts, and ZnSe·$0.5N_2H_4$ hybrid nanoflakes. We analyzed the samples by electron microscopy, UV−visible absorption, photoluminescence (PL), and time-resolved PL spectroscopy, discussed the growth mechanism, and demonstrated that the hybrid nanostructures can practically convert light into chemical energy. The optical spectroscopy data suggest that the three hybrid nanostructures were capable of effective visible light absorption and possessed relatively long exciton lifetimes, making them highly desirable for photocatalysis applications. We evaluated and compared the photocatalytic performance of the samples through the photodegradation of rhodamine B (RhB) under visible light illumination. With the substantially long exciton lifetime of 9.79 ns, ZnSe·$0.5N_2H_4$ hybrid nanowires performed much better in the photodegradation of RhB than the other counterpart samples. Further transformation into pure-phase ZnSe nanowires was also conducted by treating ZnSe·$0.5N_2H_4$ hybrid nanowires with a post-annealing or a secondary hydrothermal operation. Compared to the pure-phase ZnSe nanowires and relevant commercial products, the as-synthesized ZnSe·$0.5N_2H_4$ hybrid nanowires exhibited superior photocatalytic performance under visible light illumination, revealing their promising potential in relevant photoconversion applications.

EXPERIMENTAL SECTION

Chemicals. All the chemicals were analytic grade reagents and used without further purification.

Preparation of Hybrid Nanostructures. The synthesis was carried out in a hydrothermal reaction. In the typical procedure, $ZnCl_2$ (0.5 mmol) and Se powder (0.5 mmol) were dissolved in a mixed solution (50 mL) of hydrazine hydrate ($N_2H_4·H_2O$) and deionized water. After it was stirred at room temperature for 1 h, the reaction solution was transferred into a Teflon-lined stainless-steel autoclave (100 mL of capacity) and allowed for hydrothermal reaction at 180 °C for 12 h. The resultant precipitate was collected by centrifugation, washed with deionized water and ethanol, and then dried in vacuum for later characterizations. In this work, various volume ratios of hydrazine hydrate to deionized water ($V_{N2H4/H2O}$ = 10/40, 20/30, 30/20, 40/10) were employed to prepare nanostructures with distinct morphologies. The products were respectively characterized as ZnSe nanoparticles, ZnSe·$0.5N_2H_4$ hybrid nanowires, ZnSe·$0.5N_2H_4$ hybrid nanobelts, and ZnSe·$0.5N_2H_4$ hybrid nanoflakes.

Preparation of Pure-Phase ZnSe Nanowires. ZnSe·$0.5N_2H_4$ nanowires from the hydrothermal process were further treated with a post-annealing operation or a secondary hydrothermal reaction, which resulted in the formation of pure-phase ZnSe nanowires. For the post-annealing treatment, 20 mg of ZnSe·$0.5N_2H_4$ nanowires were annealed at 400 °C in nitrogen atmosphere for 1 h. As to the secondary hydrothermal reaction, 20 mg of ZnSe·$0.5N_2H_4$ nanowires were added to 30 mL of ethanol. The suspension was then transferred into a Teflon-lined stainless-steel autoclave (100 mL of capacity) and allowed for hydrothermal reaction at 180 °C for 24 h.

Preparation of Au-Decorated ZnSe·$0.5N_2H_4$ Nanowires. The decoration of Au particles on ZnSe·$0.5N_2H_4$ nanowires was carried out using a chemical reduction method.[17] Briefly, ZnSe·$0.5N_2H_4$ nanowires of 3.0 mg were dispersed in the reaction solution containing 60 mL of deionized water and 30 mL of ethanol, followed by the addition of a desirable amount of $HAuCl_4$ solution (10 mM). After it was stirred at 30 °C for 30 min, the suspension was centrifuged, washed, and then dried in vacuum for later use. In this work, three different volumes of $HAuCl_4$ solution were employed to produce Au-decorated ZnSe·$0.5N_2H_4$ nanowires with increasing Au content. From energy-dispersive X-ray spectrometry (EDS) analysis, the content of Au deposited on ZnSe·$0.5N_2H_4$ nanowires was respectively determined to be 5, 10, and 20 wt %.

Photocatalytic Performance Measurement. The photocatalytic activities of the samples were evaluated by monitoring the photodegradation of RhB. The optical system used for photodegradation consisted of a xenon lamp (500 W, 175 mW/cm^2) and a bandpass filter (bandwidth of 400−700 nm), which allowed the irradiation in the visible range. A quartz tube with a capacity of 30 mL was used as the photoreactor vessel. A typical experiment involved adding 5.0 mg of photocatalyst to 15 mL of RhB aqueous solution (1.0×10^{-5} M) in the photoreactor vessel. Prior to illumination, the suspension was aerated and stirred in the dark for 15 min to reach the adsorption equilibrium of RhB with photocatalyst. At certain time intervals of illumination, 1.5 mL of the reaction solution was withdrawn and centrifuged to remove photocatalyst particles. The filtrates were analyzed with a UV−visible spectrophotometer to measure the concentration variation of RhB through recording the corresponding absorbance of the characteristic peak at 581 nm. The photocatalytic data were fit to the pseudo-first-order reaction model, in which the reaction rate constant of RhB degradation can be determined. Note that methylene bule (denoted as MB) was used as the test pollutant when evaluating the photocatalytic efficiency of Au-decorated ZnSe·$0.5N_2H_4$ nanowires. The experiment was performed in the ethanolic solution of MB (15 mL, 1.0×10^{-5} M), in which ethanol was used as the sacrificial hole scavenger to facilitate the utilization of the separated electrons.[17]

Exciton Lifetime Measurement. Time-resolved PL spectra were measured using a customized single-photon counting system (Horiba Jobin Yvon) that delivers an instrument response function down to 25 ps fwhm. A GaN diode laser (λ = 375 nm) was used as the excitation source. The signals collected at the excitonic emission of the samples were dispersed by a grating spectrometer, detected by a high-speed photomultiplier tube, and then correlated using a single-photon counting card. The recorded emission decay data were analyzed and fitted with a biexponential kinetics model $I(t) = A_1e^{-t/\tau_1} + A_2e^{-t/\tau_2}$, which generates two lifetime values, τ_1 and τ_2, and the corresponding amplitudes, A_1 and A_2.[18] The intensity-average exciton lifetime, $\langle\tau\rangle$, was determined using the following expression: $\langle\tau\rangle = (A_1\tau_1^2 + A_2\tau_2^2)/(A_1\tau_1 + A_2\tau_2)$. All the fitting results were summarized in Table 1. The near-unity value of goodness (χ^2) of the fitting implied a good fit to the experimental data.

Characterization. The morphology and dimensions of the products were examined with a field-emission scanning electron microscope (SEM, JEOL JSM-6500F) and a transmission electron microscope (TEM, JEOL JEM-2010) operated at 200 kV. The crystallographic structure of the samples was investigated with X-ray diffraction (XRD, MAC Science, MXP18). The elemental analysis of the samples was conducted with EDS, the accessory of SEM (JSM-6500F) and TEM (JEM-2010). Thermogravimetric (TG) analysis was performed on a TA Instruments Q500 at a heating rate of 10 °C/min in N_2 atmosphere. X-ray photoelectron spectroscopy (XPS) measurement was conducted with a VG Scientific Microlab 350 using Mg Kα radiation under high vacuum condition. UV−visible absorption spectra

DOI: 10.1021/am507085u
ACS Appl. Mater. Interfaces 2015, 7, 1616−1623

Table 1. Kinetic analysis of emission decay for different samples

entry (I)	A_1 (%)	τ_1 (ns)	A_2 (%)	τ_2 (ns)	$\langle\tau\rangle$ (ns)	χ^2
ZnSe nanoparticles	2.6	10.62	97.4	1.50	2.94	1.00
ZnSe·0.5N_2H_4 nanowires	19.5	13.60	80.5	1.57	9.79	1.30
ZnSe·0.5N_2H_4 nanobelts	3.6	12.81	96.4	1.56	4.20	1.02
ZnSe·0.5N_2H_4 nanoflakes	3.2	12.46	96.8	1.53	3.88	1.02
entry (II)	A_1 (%)	τ_1 (ns)	A_2 (%)	τ_2 (ns)	$\langle\tau\rangle$ (ns)	χ^2
ZnSe·0.5N_2H_4 nanowires	19.5	13.60	80.5	1.57	9.79	1.30
with 5 wt % Au	18.2	11.57	81.8	1.39	7.99	1.03
with 10 wt % Au	16.2	9.80	83.8	1.36	6.27	1.03
with 20 wt % Au	15.4	9.07	84.6	1.25	5.98	1.21

were collected using a Hitachi U-3900H spectrophotometer. For steady-state PL spectroscopy, a Hitachi F-4500 equipped with a 150 W xenon lamp was used. All of the absorption and emission spectra were recorded at room temperature under ambient atmosphere.

RESULTS AND DISCUSSION

The structure and dimensions of the samples were first investigated using SEM, TEM, and XRD. Figure S1, of the Supporting Information, and Figure 1 present the SEM and

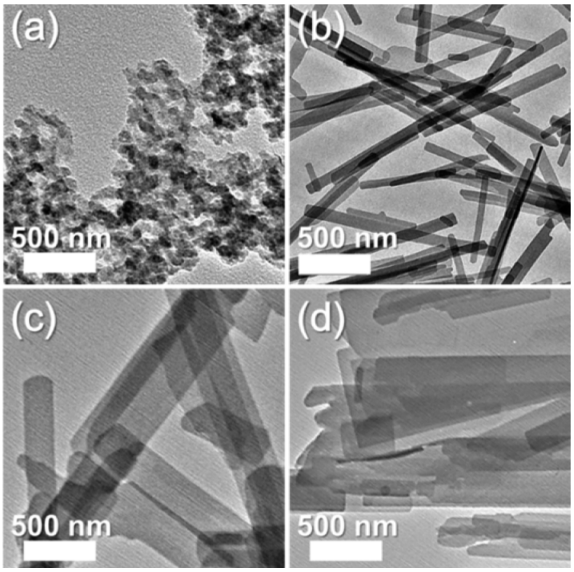

Figure 1. TEM images for the samples prepared with $V_{N2H4/H2O}$ of (a) 10/40, (b) 20/30, (c) 30/20, and (d) 40/10.

TEM images for the samples prepared with different volume ratios of hydrazine hydrate to deionized water ($V_{N2H4/H2O}$), which clearly revealed distinct nanostructures contained therein. The sample prepared with $V_{N2H4/H2O}$ of 10/40 was composed of particle aggregation with a primary particle size of 10–20 nm. The corresponding XRD pattern of Figure 2 suggested that the sample was zinc blende ZnSe. As $V_{N2H4/H2O}$ of 20/30, 30/20, and 40/10 were employed, quasi-one-dimensional nanostructures were found prevalent in the products. According to the structural features, the samples were respectively depicted as nanowires, nanobelts, and nanoflakes. The nanowires had a typical diameter of 80–100 nm and length up to a few μm, whereas the nanobelts and

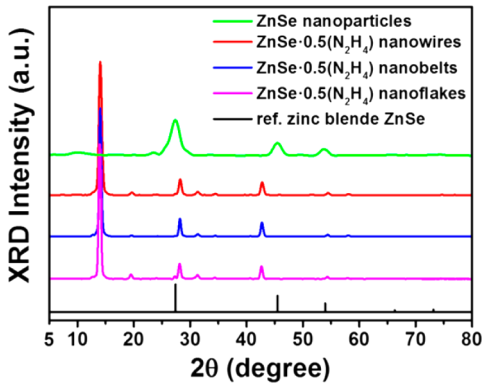

Figure 2. XRD patterns of ZnSe nanoparticles and the three ZnSe·0.5N_2H_4 hybrid nanostructures. The standard pattern of zinc blende ZnSe (JCPDS #80–0021) was also included for comparison.

nanoflakes had a relatively large width of 200–500 nm and 0.5–1.0 μm, respectively, and a comparable length. As shown in Figure 2, the three quasi-one-dimensional nanostructure samples displayed diffraction peaks that cannot be indexed to any known phase of Zn, Se, or ZnSe. Nevertheless, the position and relative intensity of the reflections were quite similar to those of ZnSe molecular precursors,[5] which were believed to have lamellar structures with ZnSe nanolayers ordered by bridging N_2H_4 spacers. In addition, there were no diffraction peaks attributable to Se, SeO_2, or other impurities, suggesting the compositional uniformity for the as-obtained samples. Here, we surmised that the three samples were composed of ZnSe layered structures with N_2H_4 orderly intercalated between the slabs. This contention was supported by the prominent diffraction peak recorded at 2θ of 14.0°, which was representative of layered structures containing organic spacers.[6] The exact composition for the three ZnSe-based hybrid samples will be later determined from TG analysis.

The growth mechanism for the distinct ZnSe-based hybrid nanostructures was proposed as follows. It has been believed that hydrazine played a crucial role in determining the morphology and composition of the inorganic–organic hybrid nanostructures containing N_2H_4 substance.[19,20] In the current hydrothermal system, hydrazine may work as reducing agent, coordination molecule, and molecular template to mediate the crystal growth of the hybrid nanostructures. With the addition of sufficient hydrazine ($V_{N2H4/H2O}$ = 10/40), Se powder could be properly reduced to generate Se^{2-} ions,[21] which enabled the reaction with Zn^{2+} to form ZnSe.[22] As the hydrazine content was further raised ($V_{N2H4/H2O}$ = 20/30, 30/20, and 40/10), hydrazine may otherwise coordinate Zn^{2+} ions to stabilize the reaction species and thus affect the reaction kinetics. Note that hydrazine is a bidentate ligand, and its coordination with Zn^{2+} can produce tetradentate complex of $[Zn(N_2H_4)_2]^{2+}$.[23] The Se^{2-} ions can then bind to the Zn^{2+} moiety of $[Zn(N_2H_4)_2]^{2+}$ by replacing part of the N_2H_4 constituents. The remaining, anchored N_2H_4 molecules subsequently induced the stacking of the neighboring ZnSe subunits via the intermolecular attraction, further leading to the formation of ZnSe layered structures with N_2H_4 orderly intercalated between each layer.[14,24] Since the subunit stacking occurred along a specific direction, the resultant nanostructures were characteristic of quasi-one-dimensional morphology. However, such subunit stacking may become less unidirectional with increasing $V_{N2H4/H2O}$ employed, as can be recognized from the morphological

DOI: 10.1021/am507085u
ACS Appl. Mater. Interfaces 2015, 7, 1616–1623

evolution from the highly anisotropically shaped nanowires ($V_{N2H4/H2O}$ = 20/30) to the nearly two-dimensionally assembled nanoflakes ($V_{N2H4/H2O}$ = 40/10).

The presence of N_2H_4 in the hybrid nanostructures was examined with TG and XPS analyses. In particular, the content of N_2H_4 for the samples from $V_{N2H4/H2O}$ = 20/30, 30/20, 40/10 was estimated by TG analysis, from which the exact composition can be determined. The three hybrid samples displayed identical TG results with a weight-loss curve quite similar to the previous reports.[22] As Figure 3a shows, the TG

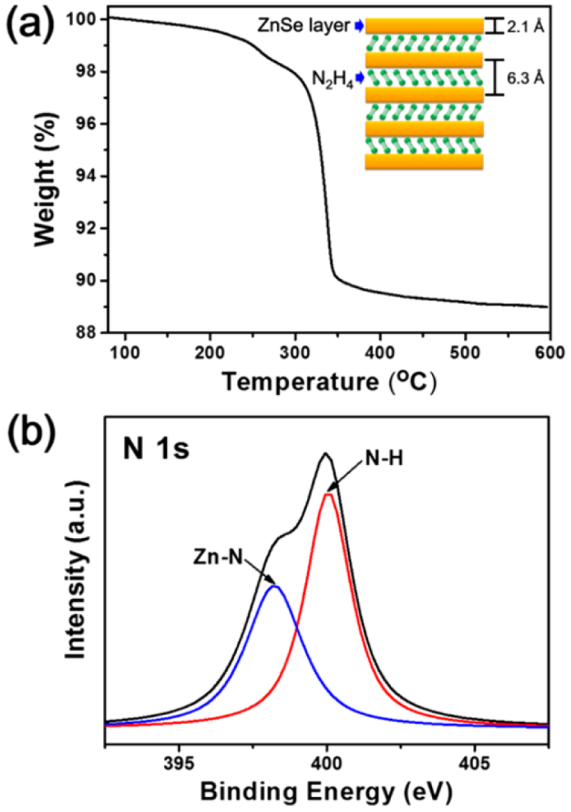

Figure 3. (a) TG analysis and (b) N 1s XPS spectrum recorded on $ZnSe{\cdot}0.5N_2H_4$ hybrid nanowires. Inset depicts the structure view for the $ZnSe{\cdot}0.5N_2H_4$ hybrid structures.

plot of the nanowire sample revealed a weight loss of 11.1% from 100 to 500 °C, which was related to the loss of the intercalated N_2H_4. On the basis of the value of weight loss, the N_2H_4 content was estimated, and the composition of the three hybrid samples was determined as $ZnSe{\cdot}0.5N_2H_4$. The inset of Figure 3a further depicts a plausible structure view for the $ZnSe{\cdot}0.5N_2H_4$ hybrid samples. According to the XRD examinations, an interlayer spacing of 6.3 Å (from 2θ = 14.0 °) along with a ZnSe monolayer thickness of 2.1 Å (from 2θ= 42.7°) was considered, quite approximate to the structural model reported for ZnSe·0.5(EN).[14,25] Note that the interlayer spacing of 6.3 Å may correspond to the distance between the two neighboring ZnSe layers. The intercalation of N_2H_4 within the ZnSe framework can be further verified by the formation of nitride constituent (Zn−N bonds) observed in the corresponding XPS analysis. In Figure 3b, the deconvolution of N 1s peak yielded two chemical states: the first component at 398.2 eV, which was assigned to the nitride constituent (Zn−N), and the second component at 400.2 eV, corresponding to the amine group (N−H) of N_2H_4.[26,27] This result, together with the findings from XRD and TG analyses, confirmed the growth of $ZnSe{\cdot}0.5N_2H_4$ hybrid nanostructures by employing a mixed solution of hydrazine hydrate and deionized water in the hydrothermal reaction.

With the ZnSe constituent serving as the structural framework, the present $ZnSe{\cdot}0.5N_2H_4$ hybrid nanostructures may receive unique material properties from ZnSe.[25] Particularly, the combination with N_2H_4 can possibly tailor the resulting optical properties, which has significant implications in the aspect of photoconversion applications. We first used steady-state PL spectroscopy to characterize the optical properties of the hybrid nanostructures. As shown in Figure 4a, the three hybrid nanostructures all exhibited an

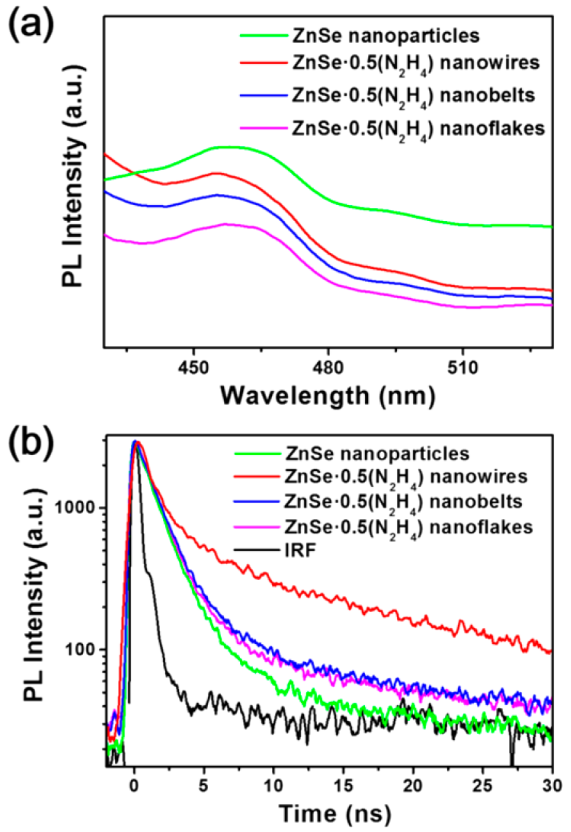

Figure 4. (a) Steady-state PL and (b) time-resolved PL spectra for ZnSe nanoparticles and the three $ZnSe{\cdot}0.5N_2H_4$ hybrid nanostructures. In (b), the instrumental response function (IRF) was also included for comparison.

unambiguous PL emission in the wavelength range of 450−480 nm. Considering its similarity to the spectrum of ZnSe nanoparticles, such an emission was ascribed to the band edge emission of the ZnSe constituent. This contention can be evidenced by the corresponding absorption spectrum (Supporting Information, Figure S2a), in which an absorption edge at ~440 nm was identified and assigned to the excitonic absorption of ZnSe. To elucidate the origin of this emission and its significance, time-resolved PL measurements were further conducted at room temperature. Specifically, the exciton lifetime derived from the time-resolved PL spectroscopy may give insightful information for evaluating the applicability of the samples. Figure 4b shows the time-resolved PL spectra of the hybrid nanostructures compared with that of pure ZnSe nanoparticles. These decay profiles were fitted with a

DOI: 10.1021/am507085u
ACS Appl. Mater. Interfaces 2015, 7, 1616−1623

biexponential function, which generates a slow (τ_1) and a fast (τ_2) decay component respectively assigned to radiative and nonradiative deactivation processes.[28] The intensity-average lifetime $\langle\tau\rangle$ was then calculated and presented to make an overall comparison of the exciton lifetime. For ZnSe nanoparticles, a considerably fast PL decay with an average exciton lifetime of 2.94 ns was recorded, signifying the fast recombination of charge carriers as expected for plain ZnSe. In contrast with ZnSe nanoparticles, the three hybrid nanostructures had rather slow emission decay, with ZnSe·0.5N_2H_4 nanowires showing the slowest decay dynamics. As noted in Table 1, the average exciton lifetime of ZnSe·0.5N_2H_4 nanowires, ZnSe·0.5N_2H_4 nanobelts, and ZnSe·0.5N_2H_4 nanoflakes was, respectively, determined to be 9.79, 4.20, and 3.88 ns. The observed slow exciton decay of the hybrid nanostructures can be attributed to the N_2H_4 intercalation, which mediated charge dynamics by confining the excitons within the ZnSe constitute.[3] A type-I straddling band alignment model was considered to account for the observed slow exciton decay. Similar to the model proposed for ZnSe·0.5(EN),[3] both the valence and conduction band edges of ZnSe were suggested to lie within the energy gap of N_2H_4. Therefore, the photoexcited charge carriers tended to be confined to ZnSe and possessed prolonged lifetimes as a result of effective surface passivation by N_2H_4. In addition, the dimensional anisotropy, which promoted electron delocalization and thus suppressed possible nonradiative recombination,[29−31] also contributed to the prolonged exciton lifetime of the hybrid nanostructures, especially for ZnSe·0.5N_2H_4 nanowires. The fact that ZnSe·0.5N_2H_4 nanowires displayed obviously increased amplitude contribution from the slow decay component (A_1 = 19.5%) may support the above proposition.

With the substantially long exciton lifetime, the present ZnSe·0.5N_2H_4 nanowires show promise for use in photoconversion applications. Importantly, the composed ZnSe was capable of harvesting visible light, making the hybrid nanostructures practical for solar energy conversion. To assess the applicability, we performed a series of photocatalysis experiments under visible light illumination by using RhB as the test pollutant. Figure 5 shows the photodegradation of RhB as a function of irradiation time over different samples. Several important features can be observed. First, as compared to N-doped P-25 TiO_2 powder[32] and ZnSe nanoparticles, the three hybrid nanostructures all exhibited better photocatalytic performance under visible light illumination. The better performance of ZnSe·0.5N_2H_4 was attributed to the dimensional anisotropy that can facilitate charge transport to enhance carrier utilization.[31] Second, among the three hybrid nanostructures tested, ZnSe·0.5N_2H_4 nanowires attained the highest photocatalytic efficiency with an apparent reaction rate constant of 0.013 min^{-1}, which is ∼1.4 and 1.9 times the value of hybrid nanobelts (0.009 min^{-1}) and hybrid nanoflakes (0.007 min^{-1}). The superior photocatalytic performance of ZnSe·0.5N_2H_4 nanowires can be accounted for by the more facile charge transport resulting from the highly anisotropic nanowire structure as well as the lasting exciton lifetime enabling the further carrier utilization. The beneficial effect of anisotropic structures on the photocatalytic performance has also been reported in TiO_2 case, in which TiO_2 nanorods with high aspect ratio showed enhanced photocatalytic activity relative to TiO_2 nanospheres.[29] Furthermore, the results of adsorption equilibrium revealed that the three hybrid samples had slightly different capability toward RhB adsorption. After stirring in the dark for 30 min, ZnSe·0.5N_2H_4 nanowires, ZnSe·0.5N_2H_4 nanobelts, and ZnSe·0.5N_2H_4 nanoflakes adsorbed 15.4, 10.5, and 11.5% of RhB, respectively. This outcome illustrated that the superior photoactivity of ZnSe·0.5N_2H_4 nanowires over nanobelts and nanoflakes was partly related to the structural effect associated with active sites and dye adsorption. Third, ZnSe·0.5N_2H_4 nanowires performed better toward RhB photodegradation than the two pure-phase ZnSe nanowires did. Here, pure-phase ZnSe nanowires were prepared by further processing ZnSe·0.5N_2H_4 nanowires with heat treatment or hydrothermal reaction, which represented the typical product obtained following the hydrazine-assisted hydrothermal process.[6,7,10,12] As Supporting Information, Figure S3 shows, the pure-phase, wurtzite ZnSe nanowires inherited the dimensions of the initial ZnSe·0.5N_2H_4. The superiority of ZnSe·0.5N_2H_4 nanowires over the pure-phase ZnSe counterpart samples may emphasize the remarkable photocatatylic properties for ZnSe·0.5N_2H_4. This outcome further illustrates that one can simply apply ZnSe·0.5N_2H_4 hybrid nanostructures to practical photoconversion processes rather than employ pure-phase ZnSe by processing ZnSe·0.5N_2H_4 with complicated procedures, which has not been realized before.

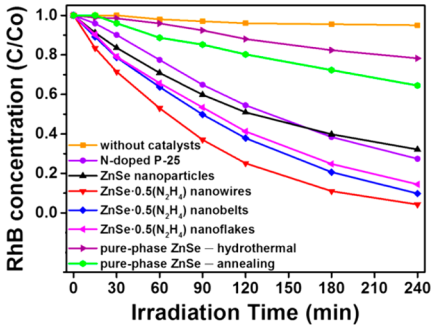

Figure 5. C/C_0 vs irradiation time plots for RhB photodegradation without any catalyst and in the presence of different samples.

To tailor the photocatalytic properties of ZnSe·0.5N_2H_4, the hybrid nanowires were further decorated with Au particles to endow them with structural and compositional diversities, a typical strategy developed for advanced photocatalytic applications.[33,34] Supporting Information, Figure S4 displays the TEM images of the resultant Au-decorated ZnSe·0.5N_2H_4 nanowires, which reveal an increase in Au particle density with increasing Au content. The surface-decorated Au may function as an effective electron acceptor for ZnSe·0.5N_2H_4 to promote charge-carrier separation, which is essential for enhancing the photocatalytic efficiency.[35−38] The charge-transfer event between ZnSe·0.5N_2H_4 and Au can be probed by monitoring the emission decay of ZnSe·0.5N_2H_4. Figure 6a shows the time-resolved PL spectra for ZnSe·0.5N_2H_4 nanowires upon the decoration of Au particles at three increasing contents. Evidently, decoration of Au reduced the exciton lifetime of ZnSe·0.5N_2H_4, suggesting the occurrence of nonradiative charge transfer from ZnSe·0.5N_2H_4 to Au. This supposition was supported by the suppressed PL emission observed for Au-decorated ZnSe·0.5N_2H_4 (Supporting Information, Figure S2b). As noted in Table 1, the average exciton lifetimes for the samples with Au content of 5, 10, and 20 wt % were, respectively, determined to be 7.99, 6.27, and 5.98 ns. The gradually decreased lifetime illustrated that charge transfer from ZnSe·0.5N_2H_4 to Au was increasingly evident for the samples

DOI: 10.1021/am507085u
ACS Appl. Mater. Interfaces 2015, 7, 1616−1623

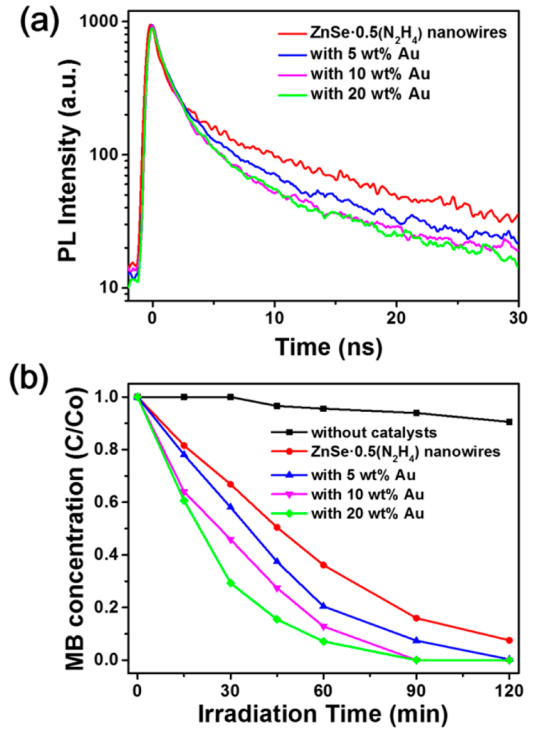

Figure 6. (a) Time-resolved PL spectra for Au-decorated ZnSe·$0.5N_2H_4$ nanowires with different Au content. (b) C/C_0 vs irradiation time plots for MB photodegradation by using different Au-decorated ZnSe·$0.5N_2H_4$ samples.

with increasing Au content. By comparing the average lifetime of the pristine ZnSe·$0.5N_2H_4$ and Au-decorated ZnSe·$0.5N_2H_4$,[39] we estimated that for the samples with 5, 10, and 20 wt % Au, approximately 18.4, 36.0, and 38.9% of the photoexcited electrons in ZnSe·$0.5N_2H_4$ were transported to Au, respectively. These separated electrons may either be collected for photocurrent generation or participate in redox reactions for photocatalysis utilization. Figure 6 clearly illustrates the beneficial effect of Au decoration on the photocatalytic properties of ZnSe·$0.5N_2H_4$ nanowires. Note that to examine the utilization of the separated electrons, MB, a cationic dye that can be decomposed by accepting electrons from the irradiated photocatalysts,[40,41] was used as the test pollutant for Au-decorated ZnSe·$0.5N_2H_4$ nanowires. The results showed that the photocatalytic efficiency of ZnSe·$0.5N_2H_4$ nanowires toward MB degradation was significantly enhanced upon the decoration of Au particles. The enhancement was ascribed to the deposited Au that can promote the overall charge separation by readily accepting photoexcited electrons from ZnSe·$0.5N_2H_4$, therefore providing more electrons for the decomposition of MB. This demonstration reveals that the ZnSe·$0.5N_2H_4$ hybrid nanostructures may serve as a versatile photocatalyst platform for advanced photocatalytic applications. On the other hand, the plasmonic effect,[42] in which nanosized Au may sensitize semiconductor nanocrystals via surface plasmon resonance, also needs to be considered. As displayed in Supporting Information, Figure S2a, the Au-decorated ZnSe·$0.5N_2H_4$ nanowires showed an additional absorption band at ~570 nm. This band can be attributed to the typical surface plasmon resonance absorption that originated from the decorated Au. Since the surface plasmon resonance absorption was evident, the plasmonic effect and its involvement in photocatalysis cannot be ruled out at the current stage.

CONCLUSIONS

In conclusion, ZnSe·$0.5N_2H_4$ hybrid nanostructures with distinct morphologies have been prepared by a facile hydrazine-assisted hydrothermal route in a mixed solvent system containing a variable volume ratio of hydrazine hydrate to water. The reaction medium consisting of mixed solvents played an important role in dictating the morphology of the products. All of the three ZnSe·$0.5N_2H_4$ hybrid nanostructures exhibited prominent band edge emission at 465 nm with a rather long exciton lifetime, making them desirable for photocatalytic applications. Among the three hybrid nanostructures tested, ZnSe·$0.5N_2H_4$ nanowires attained the highest photocatalytic efficiency toward RhB degradation, which can be accounted for by the more facile charge transport resulting from the highly anisotropic nanowire structure as well as the lasting exciton lifetime (9.79 ns) enabling the further carrier utilization. As compared to pure ZnSe nanoparticles and single-phase ZnSe nanowires obtained from further processing ZnSe·$0.5N_2H_4$, the ZnSe·$0.5N_2H_4$ hybrid nanowires exhibited superior photocatalytic performance under visible light illumination. A further enhancement in the photocatalytic activity can be achieved for ZnSe·$0.5N_2H_4$ hybrid nanowires when Au particles of desirable amount were deposited on their surfaces. The demonstrations from this work may facilitate the use of semiconductor-based inorganic−organic hybrid nanostructures in practical photoconversion processes. Particularly, the synergy between the inorganic and organic constituents has further implications for modulating the interfacial charge transfer and enhancing the light harvesting, both of which are considered essential for pushing forward the advancement of photocatalyst technology.

ASSOCIATED CONTENT

Supporting Information

SEM images, UV−visible absorption spectra, PL emission spectra, XRD patterns, TEM images and TEM-EDS result of the samples. This material is available free of charge via the Internet at http://pubs.acs.org.

AUTHOR INFORMATION

Corresponding Author

*E-mail: yhsu@cc.nctu.edu.tw.

Author Contributions

†Y.-C. Chen and T.-C. Liu contributed equally to this work.

Notes

The authors declare no competing financial interest.

ACKNOWLEDGMENTS

This work was financially supported by the Ministry of Science and Technology of Republic of China (Taiwan) under Grants Nos. NSC-102-2113-M-009-005-MY2 and NSC-102-3113-P-009-002.

REFERENCES

(1) Zhang, X.; Hejazi, M.; Thiagarajan, S. J.; Woerner, W. R.; Banerjee, D.; Emge, T. J.; Xu, W.; Teat, S. J.; Gong, Q.; Safari, A.; Yang, R.; Parise, J. B.; Li, J. From 1D Chain to 3D Network: A New Family of Inorganic−Organic Hybrid Semiconductors $MO_3(L)_x$ (M =

DOI: 10.1021/am507085u
ACS Appl. Mater. Interfaces 2015, 7, 1616−1623

Mo, W; L = Organic Linker) Built on Perovskite-like Structure Modules. *J. Am. Chem. Soc.* **2013**, *135*, 17401−17407.
(2) Lu, J.; Wei, S.; Yu, W.; Zhang, H.; Qian, Y. Structure and Luminescence of 2D Dilute Magnetic Semiconductors: $Cd_{1-x}Mn_xSe{\cdot}L_{0.5}$ (L = Diamines). *Chem. Mater.* **2005**, *17*, 1698−1703.
(3) Zhang, Y.; Dalpian, G. M.; Fluegel, B.; Wei, S.-H.; Mascarenhas, A.; Huang, X.-Y.; Li, J.; Wang, L.-W. Novel Approach to Tuning the Physical Properties of Organic-Inorganic Hybrid Semiconductors. *Phys. Rev. Lett.* **2006**, *96*, 026405.
(4) Su, Y.-W.; Lin, W.-H.; Hsu, Y.-J.; Wei, K.-H. Conjugated Polymer/Nanocrystal Nanocomposites for Renewable Energy Applications in Photovoltaics and Photocatalysis. *Small* **2014**, *10*, 4427−4442.
(5) Kim, J.-Y.; Kim, M. R.; Park, S.-Y.; Jang, D. J. Hydrothermal Growth Control of $ZnSe{\cdot}N_2H_4$ Nanobelts. *CrystEngComm* **2010**, *12*, 1803−1808.
(6) Yang, J.; Wang, G.; Liu, H.; Park, J.; Gou, X.; Cheng, X. Solvothermal Synthesis and Characterization of ZnSe Nanoplates. *J. Cryst. Growth* **2008**, *310*, 3645−3648.
(7) Wang, H.; Tian, T.; Yan, S.; Huang, N.; Xiao, Z. Large-scale Synthesis of ZnSe Nanoribbons on Zinc Substrate. *J. Cryst. Growth* **2009**, *311*, 3787−3791.
(8) Zhang, Y.; Hu, C.; Feng, B.; Wang, X.; Wan, B. Synthesis and Photocatalytic Property of ZnSe Flowerlike Hierarchical Structure. *Appl. Surf. Sci.* **2011**, *257*, 10679−10685.
(9) Kole, A. K.; Tiwary, C. S.; Kumbhakar, P. Ethylenediamine Assisted Synthesis of Wurtzite Zinc Sulphide Nanosheets and Porous Zinc Oxide Nanostructures: Near White Light Photoluminescence Emission and Photocatalytic Activity under Visible Light Irradiation. *CrystEngComm* **2013**, *15*, 5515−5525.
(10) Yao, W.; Yu, S.-H.; Huang, X.; Jiang, J.; Zhao, L. Q.; Pan, L.; Li, J. Nanocrystals of an Inorganic−Organic Hybrid Semiconductor: Formation of Uniform Nanobelts of $[ZnSe](Diethylenetriamine)_{0.5}$ in a Ternary Solution. *Adv. Mater.* **2005**, *17*, 2799−2802.
(11) Mitzi, D. B. Polymorphic One-Dimensional $(N_2H_4)_2ZnTe$: Soluble Precursors for the Formation of Hexagonal or Cubic Zinc Telluride. *Inorg. Chem.* **2005**, *44*, 7078−7086.
(12) Xi, B.; Xiong, S.; Xu, D.; Li, J.; Zhou, H.; Pan, J.; Li, J.; Qian, Y. Tetraethylenepentamine-Directed Controllable Synthesis of Wurtzite ZnSe Nanostructures with Tunable Morphology. *Chem.—Eur. J.* **2008**, *14*, 9786−9791.
(13) Yu, S.-H.; Wu, Y.-S.; Yang, J.; Han, Z.-H.; Xie, Y.; Qian, Y.-T.; Liu, X.-M. A Novel Solventothermal Synthetic Route to Nanocrystalline CdE (E = S, Se, Te) and Morphological Control. *Chem. Mater.* **1998**, *10*, 2309−2312.
(14) Deng, Z.-X.; Li, L.; Li, Y. Novel Inorganic-Organic-Layered Structures: Crystallographic Understanding of Both Phase and Morphology Formations of One-Dimensional CdE (E = S, Se, Te) Nanorods in Ethylenediamine. *Inorg. Chem.* **2003**, *42*, 2331−2341.
(15) Yao, W.-T.; Yu, S.-H. Synthesis of Semiconducting Functional Materials in Solution: From II-VI Semiconductor to Inorganic−Organic Hybrid Semiconductor Nanomaterials. *Adv. Funct. Mater.* **2008**, *18*, 3357−3366.
(16) Zhou, G. T.; Wang, X.; Yu, J. C. A Low-Temperature and Mild Solvothermal Route to the Synthesis of Wurtzite-Type ZnS with Single-Crystalline Nanoplate-like Morphology. *Cryst. Growth Des.* **2005**, *5*, 1761−1765.
(17) Pu, Y.-C-; Chen, Y.-C.; Hsu, Y.-J. Au-decorated $Na_xH_{2-x}Ti_3O_7$ Nanobelts Exhibiting Remarkable Photocatalytic Properties under Visible-Light Illumination. *Appl. Catal., B* **2010**, *97*, 389−397.
(18) Williams, G.; Kamat, P. V. Graphene-Semiconductor Nanocomposites: Excited-State Interactions between ZnO Nanoparticles and Graphene Oxide. *Langmuir* **2009**, *25*, 13869−13873.
(19) Kumar, P.; Singh, K. Wurtzite ZnSe Quantum Dots: Synthesis, Characterization and PL Properties. *J. Optoelectron. Biomed. Mater.* **2009**, *1*, 59−69.
(20) Dong, Y.; Peng, Q.; Li, Y. Semiconductor Zinc Chalcogenides Nanofibers from 1-D Molecular Precursors. *Inorg. Chem. Commun.* **2004**, *7*, 370−373.
(21) Benzing, W. C.; Conn, J. B.; Magee, J. V.; Sheehan, E. J. Synthesis of Selenides and Tellurides. I. The Reduction of Selenites by Hydrazine. *J. Am. Chem. Soc.* **1958**, *80*, 2657−2659.
(22) Chen, M.; Gao, L. Synthesis and Characterization of Wurtzite ZnSe One-Dimensional Nanocrystals through Molecular Precursor Decomposition by Solvothermal Method. *Mater. Chem. Phys.* **2005**, *91*, 437−441.
(23) Bazarganipour, M.; Salavati-Niasari, M. Fabrication and Characterisation of Nanostructure Zinc Telluride by the Hydrothermal Method. *Micro Nano Lett.* **2012**, *7*, 388−391.
(24) Liu, Y.; Cao, J.; Li, C.; Zeng, J.; Tang, K.; Qian, Y.; Zhang, W. Hydrazine Route to One-Dimensional Structuralmetal Selenides Crystals. *J. Cryst. Growth* **2004**, *261*, 508−513.
(25) Heulings, H. R., IV; Huang, X.; Li, J.; Yuen, T.; Lin, C. L. Mn-Substituted Inorganic-Organic Hybrid Materials Based on ZnSe: Nanostructures that May Lead to Magnetic Semiconductors with a Strong Quantum Confinement Effect. *Nano Lett.* **2001**, *1*, 521−525.
(26) Xiao, Z.; Liu, Y.; Zhang, J.; Zhao, D.; Lu, Y.; Shen, D.; Fan, X. Electrical and Structural Properties of p-type ZnO:N Thin Films Prepared by Plasma Enhanced Chemical Vapour Deposition. *Semicond. Sci. Technol.* **2005**, *20*, 796−800.
(27) Cao, P.; Zhao, D. X.; Zhang, J. Y.; Shen, D. Z.; Lu, Y. M.; Yao, B.; Li, B. H.; Bai, Y.; Fan, X. W. Optical and Electrical Properties of p-type ZnO Fabricated by NH_3 Plasma Post-Treated ZnO Thin Films. *Appl. Surf. Sci.* **2008**, *254*, 2900−2904.
(28) Wheeler, D. A.; Zhang, J. Z. Exciton Dynamics in Semiconductor Nanocrystals. *Adv. Mater.* **2013**, *25*, 2878−2896.
(29) Yun, H. J.; Lee, H.; Joo, J. B.; Kim, W.; Yi, J. Influence of Aspect Ratio of TiO_2 Nanorods on the Photocatalytic Decomposition of Formic Acid. *J. Phys. Chem. C* **2009**, *113*, 3050−3055.
(30) Mor, G. K.; Shankar, K.; Paulose, M.; Varghese, Q. K.; Grimes, C. A. Use of Highly-Ordered TiO_2 Nanotube Arrays in Dye-Sensitized Solar Cells. *Nano Lett.* **2006**, *6*, 215−218.
(31) Wolcott, A.; Smith, W. A.; Kuykendall, T. R.; Zhao, Y.; Zhang, J. Z. Photoelectrochemical Water Splitting Using Dense and Aligned TiO_2 Nanorod Arrays. *Small* **2009**, *5*, 104−111.
(32) Cong, Y.; Zhang, J.; Chen, F.; Anpo, M. Synthesis and Characterization of Nitrogen-Doped TiO_2 Nanophotocatalyst with High Visible Light Activity. *J. Phys. Chem. C* **2007**, *111*, 6976−6982.
(33) Zhang, N.; Liu, S.; Xu, Y.-J. Recent Progress on Metal Core@Semiconductor Shell Nanocomposites as a Promising Type of Photocatalyst. *Nanoscale* **2012**, *4*, 2227−2238.
(34) Wang, H.; Zhang, L.; Chen, Z.; Hu, J.; Li, S.; Wang, Z.; Liu, J.; Wang, X. Semiconductor Heterojunction Photocatalysts: Design, Construction, and Photocatalytic Performances. *Chem. Soc. Rev.* **2014**, *43*, 5234−5244.
(35) Chen, W.-T.; Lin, Y.-K.; Yang, T.-T.; Pu, Y.-C.; Hsu, Y.-J. Au/ZnS Core/Shell Nanocrystals as an Efficient Anode Photocatalyst in Direct Methanol Fuel Cells. *Chem. Commun.* **2013**, *49*, 8486−8488.
(36) Chen, W.-T.; Hsu, Y.-J. L-Cysteine-Assisted Growth of Core-Satellite ZnS-Au Nanoassemblies with High Photocatalytic Efficiency. *Langmuir* **2010**, *26*, 5918−5925.
(37) Yang, T.-T.; Chen, W.-T.; Hsu, Y.-J.; Wei, K.-H.; Lin, T.-Y.; Lin, T.-W. Interfacial Charge Carrier Dynamics in Core-Shell Au-CdS Nanocrystals. *J. Phys. Chem. C* **2010**, *114*, 11414−11420.
(38) Chen, W.-T.; Yang, T.-T.; Hsu, Y.-J. Au-CdS Core-Shell Nanocrystals with Controllable Shell Thickness and Photoinduced Charge Separation Property. *Chem. Mater.* **2008**, *20*, 7204−7206.
(39) Harris, C.; Kamat, P. V. Photocatalytic Events of CdSe Quantum Dots in Confined Media. Electrodic Behavior of Coupled Platinum Nanoparticles. *ACS Nano* **2010**, *4*, 7321−7330.
(40) Kobasa, I. M.; Tarasenko, G. P. Photocatalysis of Reduction of the Dye Methylene Blue by Bi_2S_3/CdS Nanocomposites. *Theor. Exp. Chem.* **2002**, *38*, 255−258.
(41) Kobasa, I. M.; Kondrat'eva, I. V.; Gnatyuk, Yu. I. Photocatalytic Reduction of Methylene Blue by Formaldehyde in the Presence of Titanium Dioxide and Cadmium Sulfide Sensitized by (1-phenyl-5,6-benzoquinoline-2)-2,4-dihydroxystyryl Iodide. *Theor. Exp. Chem.* **2008**, *44*, 42−47.

DOI: 10.1021/am507085u
ACS Appl. Mater. Interfaces 2015, 7, 1616−1623

(42) Pu, Y.-C.; Wang, G.; Chang, K.-D.; Ling, Y.; Lin, Y.-K.; Fitzmorris, B. C.; Liu, C.-M.; Lu, X.; Tong, Y.; Zhang, J. Z.; Hsu, Y.-J.; Li, Y. Au Nanostructure-Decorated TiO_2 Nanowires Exhibiting Photoactivity Across Entire UV-Visible Region for Photoelectrochemical Water Splitting. *Nano Lett.* **2013**, *13*, 3817−3823.

DOI: 10.1021/am507085u
ACS Appl. Mater. Interfaces 2015, 7, 1616−1623